

A SIGNATURE OF PLANETARY MIGRATION: THE ORIGIN OF ASYMMETRIC CAPTURE IN THE 2:1 RESONANCE

RUTH A. MURRAY-CLAY¹ & EUGENE I. CHIANG^{1,2}

ACCEPTED TO APJ: September 30, 2004

ABSTRACT

The spatial distribution of Kuiper belt objects (KBOs) in 2:1 exterior resonance with Neptune constrains that planet’s migration history. Numerical simulations demonstrate that fast planetary migration generates a larger population of KBOs trailing rather than leading Neptune in orbital longitude. This asymmetry corresponds to a greater proportion of objects caught into asymmetric resonance such that their resonance angles, ϕ , librate about values $> \pi$ (trailing) as opposed to $< \pi$ (leading). We provide, for the first time, an explanation of this phenomenon, using physical, analytic, and semi-analytic arguments. Central to our understanding is how planetary migration shifts the equilibrium points of the superposed direct and indirect potentials. Symmetric libration, in which ϕ librates about $\sim \pi$, precedes capture into asymmetric resonance. As a particle transitions from symmetric to asymmetric libration, if ϕ exceeds its value, ψ , at the unstable point of asymmetric resonance, then the particle is caught into trailing resonance, while if $\phi < \psi$, the particle is caught into leading resonance. The probability that the KBO is caught into trailing resonance is determined by the fraction of time it spends with $\phi > \psi$ while in symmetric libration. This fractional time increases with faster migration because migration not only shifts ψ to values $< \pi$, but also shifts the stable point of symmetric libration to values $> \pi$. Smaller eccentricities prior to capture strengthen the effect of these shifts. Large capture asymmetries appear for exponential timescales of migration, τ , shorter than $\sim 10^7$ yr. The observed distribution of 2:1 KBOs (2 trailing and 7 leading) excludes $\tau \leq 10^6$ yr with 99.65% confidence.

Subject headings: celestial mechanics—Kuiper belt—comets: general—minor planets, asteroids

1. INTRODUCTION

Transfers of energy and angular momentum between disks and bodies embedded within them can explain a variety of observed dynamical architectures. For example, the tight orbits of close-in, extra-solar, Jovian-mass planets (“hot Jupiters”) are thought to be a consequence of orbital migration driven by parent disks composed either of viscous gas (e.g., Ward 1997) or planetesimals (e.g., Murray et al. 1998). Capture of bodies into mean-motion resonances is a celebrated signature of migration (see, e.g., Peale 1986, and references therein), showcased recently by the pair of planets orbiting GJ 876 in a 2:1 resonance (Marcy et al. 2001; Lee & Peale 2002). Migration finds application in the solar system as well; it promises to explain the preponderance of highly eccentric Kuiper belt objects (KBOs) trapped in mean-motion resonances with Neptune (Malhotra 1995; Chiang et al. 2003ab). The outermost planet in our solar system might have migrated several AUs outward by gravitationally scattering planetesimals (Fernandez & Ip 1984; Hahn & Malhotra 1999), thereby sweeping its exterior resonances across the primordial Kuiper belt and filling them with KBOs (Malhotra 1995; Chiang & Jordan 2002).

Notwithstanding the numerous appeals to disk-driven migration, it has been difficult to dispel all doubt regarding its relevance. Worries are perhaps most naggingly persistent in the Kuiper belt, where the abun-

dance of resonant KBOs could, in principle, be explained by the following stability argument. One imagines that the entire belt was once indiscriminately, dynamically excited to large eccentricities and inclinations by one or more massive perturbers—perhaps Neptune itself, during that planet’s high eccentricity phase (Goldreich, Lithwick, & Sari 2004; see also Thommes, Duncan, & Levison 1999, 2002)—and that only KBOs fortunate enough to be kicked into resonances enjoyed the phase protection that permits survival for the age of the solar system.

Chiang & Jordan (2002, hereafter CJ) propose one test of the migration hypothesis that helps to break degeneracies of interpretation. They find that in scenarios where Neptune’s migration is comparatively fast—occurring on timescales shorter than 10^7 yr, for their chosen initial conditions—more objects are caught into the 2:1 resonance with mean libration angles greater than π . This asymmetry in the distribution of libration angles manifests itself as an asymmetry on the sky: at a given epoch, more 2:1 resonant objects will appear at longitudes trailing, rather than leading, Neptune’s. This is a prediction of the migration model that can be tested observationally by wide-angle, astrometric surveys such as, e.g., Pan-STARRS (Panoramic Survey Telescope & Rapid Response System). Under either the alternative stability hypothesis or the hypothesis that Neptune’s migration occurred over timescales longer than 10^7 yr, we would expect equal populations trailing and leading Neptune.

The capture asymmetry discovered by CJ—witnessed also in numerical simulations by Wyatt (2003) in the context of debris disks molded by migrating extra-solar planets—arose from a purely numerical orbital integration. In this paper, we explain the capture asymmetry on

¹ Center for Integrative Planetary Sciences, Astronomy Department, University of California at Berkeley, Berkeley, CA 94720, USA

² Alfred P. Sloan Research Fellow
Electronic address: rmurray@astron.berkeley.edu, echiang@astron.berkeley.edu

physical grounds, using a variety of qualitative, analytic, and numerical descriptions. In uncovering the workings of the capture asymmetry on a step-by-step, mechanistic basis, we gain insight into its applicability to observations. Our focus is on the Kuiper belt, but the setting is clearly generalizable.

Terminology in this field can be confusing; we lay down some definitions here. The exterior 2:1 resonance is distinguished in offering the possibility of multiple stable points for the resonance angle,

$$\phi \equiv 2\lambda - \lambda_N - \varpi, \quad (1)$$

where λ and λ_N are the mean longitudes of the test particle (KBO) and the planet (Neptune), respectively, and ϖ is the longitude of pericenter of the particle.³ At moderate eccentricities of the particle, the angle ϕ can librate (oscillate with bounded amplitude) about a range of values. Particles whose libration centers do not equal π are said to be in “asymmetric resonance” or “asymmetric libration” (Message 1958; Frangakis 1973; Beaugé 1994; Malhotra 1996; Winter & Murray 1997; Pan & Sari 2004, and references therein). The usual libration of ϕ about π is called “symmetric resonance.” We explain the physical origins of symmetric and asymmetric resonance in §2. We refer to the migration-induced preference for objects to be caught into asymmetric resonance such that they librate about angles greater than π as “asymmetric capture.” Note that asymmetric capture does not refer merely to capture into asymmetric resonance. We explain the mechanics underlying asymmetric capture in §3. Connections to observations are made in §4, and a summary and outlook for future work are presented in §5.

2. THE ORIGIN OF ASYMMETRIC LIBRATION

We begin by explaining the origin of asymmetric libration in a static 2:1 resonant potential. Our analysis of this special case of the circular, restricted, planar 3-body problem lays the foundation for understanding the more complicated situation in which the planet is migrating. We offer two viewpoints: a physical, qualitative description in terms of impulses imparted to the particle over a synodic period (§2.1), and a graphical, quantitative interpretation using contour plots of constant Hamiltonian (§2.2).

Many of the ideas contained in this section are not new; they may be traced in various forms in pioneering work on asymmetric resonance by Message (1958), Frangakis (1973), Beaugé (1994), Malhotra (1996), Winter & Murray (1997), and Pan & Sari (2004). In particular, Frangakis (1973) and Pan & Sari (2004) highlight the key role played by the indirect potential. Pan & Sari (2004) additionally offer physical explanations of asymmetric resonance, concentrating on the large eccentricity limit and on how impulsive torques imparted to the particle near its periapsis by the central mass and by the perturber can balance. We focus instead on the regime of small-to-moderate eccentricities. Our methodology owes more to that of Peale (1986). We proceed with our version of the facts in the spirit of pedagogy and to establish

the language in which we will describe the dynamics of asymmetric resonance when the perturber migrates (§3), a subject which seems to have received much less attention.

2.1. Physical Interpretation of the Direct and Indirect Potentials

Asymmetric libration results from the superposition of the direct and indirect disturbing potentials. Consider the interaction between the Sun, Neptune, and a massless KBO in a reference frame centered on the Sun. Denote the mass of the Sun by m_\odot , the mass of the planet by m_N , the distance between the Sun and the planet by \mathbf{r}_N , and the distance between the Sun and the test particle by \mathbf{r} . Then the acceleration of the KBO equals

$$\ddot{\mathbf{r}} = \nabla_{\mathbf{r}}(U_{\text{Kep}} + R), \quad (2)$$

where

$$U_{\text{Kep}} = \frac{Gm_\odot}{|\mathbf{r}|} \quad (3)$$

is the Keplerian potential felt by the KBO, and

$$R = R_{\text{direct}} + R_{\text{indirect}} = \frac{Gm_N}{|\mathbf{r} - \mathbf{r}_N|} - \frac{Gm_N \mathbf{r}_N \cdot \mathbf{r}}{|\mathbf{r}_N|^3} \quad (4)$$

is the disturbing or perturbation potential due to the planet. Here $\nabla_{\mathbf{r}}$ is the gradient with respect to \mathbf{r} . The perturbation potential divides into a direct part, $Gm_N/|\mathbf{r} - \mathbf{r}_N|$, which governs the direct attraction between the planet and the test particle, and an indirect part, $-Gm_N \mathbf{r}_N \cdot \mathbf{r}/|\mathbf{r}_N|^3$, which accounts for the acceleration of the reference frame due to Neptune’s acceleration of the Sun. Note that in an arbitrary accelerating reference frame, there is no guarantee that the acceleration of a body can be written as the gradient of a potential. We are able to do so because the acceleration of our reference frame corresponds to the gravitational acceleration of the Sun by Neptune.

We describe the evolution of the test particle’s orbit inside the exterior 2:1 resonance in terms of its resonance angle, $\phi = 2\lambda - \lambda_N - \varpi$. The angle ϕ is approximately the angle of the line drawn through the planet and the particle at conjunction, measured from pericenter. This geometric interpretation is only approximate because ϕ is written in terms of mean longitudes rather than true longitudes.

Peale (1986) describes how ϕ evolves under the direct perturbation, and we summarize his analysis here. From conjunction to opposition, the direct perturbation adds angular momentum to the KBO through the azimuthal acceleration exerted by Neptune. From opposition to the next conjunction, the azimuthal acceleration removes angular momentum. Over a synodic period, the sign of the effect of the direct perturbation on ϕ can be decided by examining interactions near conjunction, when Neptune and the KBO are closest. Consider conjunctions at point A of Figure 1, en route from pericenter to apocenter ($0 < \phi < \pi$). The angular momentum removed from the KBO before conjunction exceeds the angular momentum imparted after conjunction for two reasons. First, the two orbits are diverging at point A. Second, the difference in angular velocities of Neptune and of the KBO is smaller before conjunction than after, so that the two bodies spend more time close to each other before conjunction. The net effect of the conjunction is therefore to

³ We label $p:q$ resonances such that $p > q$ refers to exterior resonances (outside the perturber) and $p < q$ refers to interior resonances (inside the perturber). This choice runs counter to convention, but seems commonplace in the Kuiper belt literature.

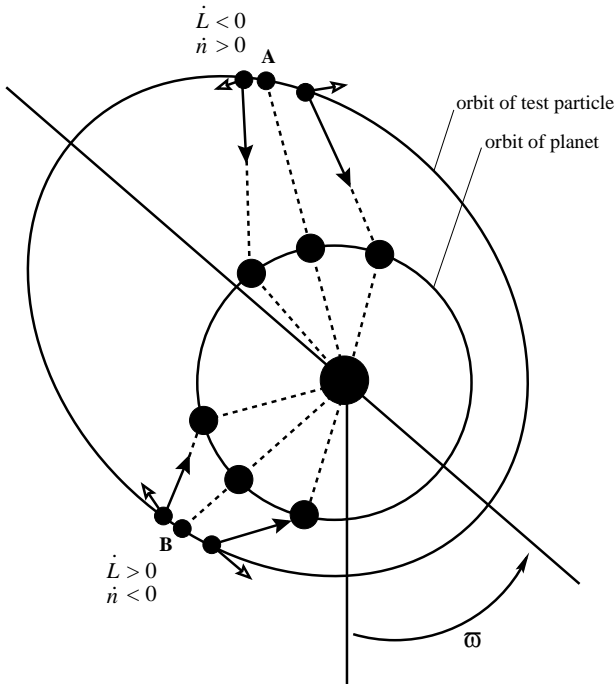


FIG. 1.— Schematic diagram of the effect of the direct disturbing potential when conjunctions occur at points A and B (not to scale). Solid arrows represent direct accelerations of the particle by the planet. Open arrows are the azimuthal components of these accelerations. The angular momentum and mean motion of the test particle are L and n , respectively. Conjunctions at point A ($0 < \phi < \pi$) remove angular momentum from the test particle, increase its mean motion, and accelerate ϕ . Conjunctions at point B result in opposite behavior. After figure 1 of Peale (1986).

pull the KBO backwards along its orbit, removing its orbital angular momentum. Its semi-major axis decreases, and its mean motion increases.⁴ As a result, the next conjunction occurs later than it would if the planet and the test particle were non-interacting; in other words, if $0 < \phi < \pi$, the direct potential increases ϕ over its value in the absence of the direct perturbation. We can say that ϕ is accelerated to larger values. Analogous considerations apply to conjunctions at point B in Figure 1 ($\pi < \phi < 2\pi$); Neptune adds angular momentum to the orbit of the KBO and ϕ decelerates.

The tendency of the direct perturbation to restore ϕ towards π is analogous to the effect of a gravitational field on the motion of a pendulum, with $\phi = \pi$ and $\phi = 0$ corresponding to the stable and unstable equilibrium points, respectively.

To understand asymmetric libration, we extend Peale’s qualitative description to encompass the effect of the indirect perturbation. As is true for the direct acceleration, the azimuthal component dominates the evolution of ϕ . Consider an infinite line connecting the Sun and the test particle. We refer to the side of this line toward which the test particle is moving as “ahead” of the KBO and to the opposite side of the line as “behind.” From conjunction to opposition, Neptune is ahead of the KBO and therefore pulls the Sun ahead of the KBO. As a result, in

⁴ This argument neglects changes in the semi-major axis of the particle due to the radial component of the direct acceleration; these changes are smaller than those brought about by the azimuthal acceleration by of order the eccentricity of the particle.

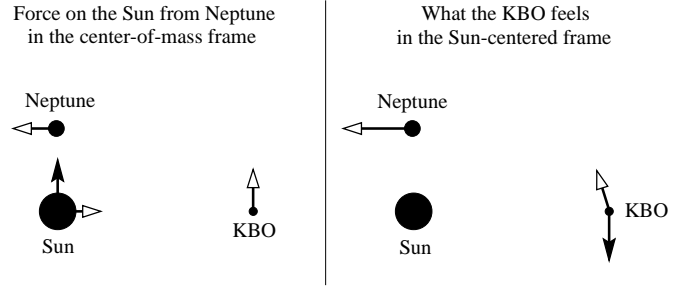


FIG. 2.— The effect of the indirect potential. Open arrows indicate the directions that bodies are moving in their orbits. Solid arrows indicate accelerations. When Neptune accelerates the Sun in an inertial reference frame (left), the KBO feels a fictitious acceleration in the opposite direction in the Sun-centered frame (right). Here Neptune is shown ahead of the KBO; in the Sun-centered frame, the indirect torque removes angular momentum from the KBO.

the Sun-centered frame, the KBO feels a fictitious torque which removes angular momentum from its orbit (Figure 2). Likewise, from opposition to the next conjunction, the fictitious indirect torque adds angular momentum to the KBO’s orbit. Integrated over the synodic period, the azimuthal component of the indirect acceleration equals

$$\langle T \rangle = -\frac{Gm_N}{a_N^2} \oint \sin \Delta\theta dt, \quad (5)$$

where $\Delta\theta \equiv \lambda_N - f - \varpi$ is the angle between the true longitude, λ_N , of the planet and the true longitude, $f + \varpi$, of the particle. For $0 < \phi < \pi$, Neptune spends more time behind the KBO, and $\langle T \rangle$ is positive;⁵ the angular momentum of the KBO in the Sun-centered frame increases, and ϕ decelerates (Figure 3). For $\pi < \phi < 2\pi$, ϕ accelerates. Thus, the indirect potential restores ϕ toward 0.

Whereas ϕ responds to the direct perturbation like a pendulum, it responds to the indirect perturbation like a metronome. The direct and indirect accelerations oppose one another; they can be balanced, forming stable points at values of ϕ intermediate between 0 and π , and intermediate between π and 2π . This balance underlies the phenomenon of asymmetric libration.

In contrast, for the 3:2 resonance, Neptune spends the same amount of time behind and ahead of the KBO regardless of the value of its (appropriately defined) resonance angle, and the indirect torque averages to zero (see §5 for a proof). Consequently, asymmetric libration is impossible for the 3:2 resonance.

2.2. Contours of Constant Hamiltonian

The long-term evolution of the KBO’s orbit when Neptune’s orbit is not varying can be summarized neatly using a Hamiltonian formulation.⁶ We seek to write down a

⁵ The time spent by Neptune forward and backward of the KBO does not alone determine the sign of $\langle T \rangle$; one must examine the exact shape of $\sin \Delta\theta$ over a synodic period. However, for the 2:1 resonance, the shape does not alter the sign of our argument. We show in §5 that $\langle T \rangle = -(Gm_N/a_N^2)\pi c_1$ for the 2:1 resonance; $c_1 < 0$ when $0 < \phi < \pi$, and $c_1 > 0$ when $\pi < \phi < 2\pi$.

⁶ We are allowed to use Hamilton’s equations with the potential $V = U_{\text{Kep}} + R$ because we can write all of the fictitious forces felt in our accelerating frame as gradients of fictitious potentials that depend only on the canonical coordinates, not the canonical

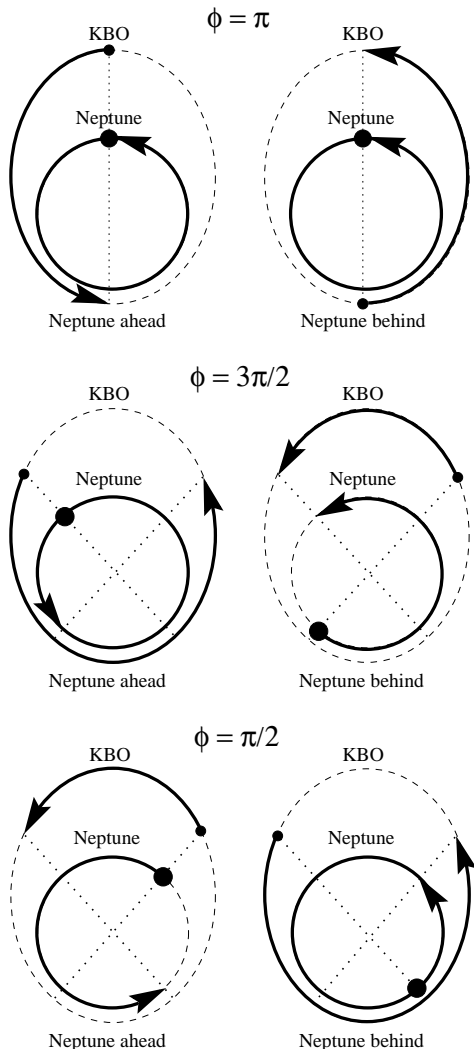


FIG. 3.— Portions of the synodic period with Neptune leading and following the KBO for $\phi = \pi$, $\pi < \phi < 2\pi$, and $0 < \phi < \pi$ (top, middle, and bottom, respectively). Solid circles indicate starting positions and arrow tips indicate ending positions. For example, if $\phi = 3\pi/2$, Neptune spends more time ahead of rather than behind the particle.

Hamiltonian having no explicit time-dependence so that we can plot level diagrams of the Hamiltonian and trace the evolution of ϕ graphically. We will make these plots in two ways, using exact (§2.2.1) and series-expanded (§2.2.2) versions of the Hamiltonian.

2.2.1. Exact Hamiltonian

We employ the Poincaré coordinates,

$$\lambda = M + \varpi, \quad \gamma = -\varpi, \quad (6)$$

and corresponding momenta,

$$\Lambda = \sqrt{\mu a}, \quad \Gamma = \sqrt{\mu a}(1 - \sqrt{1 - e^2}), \quad (7)$$

where λ is the mean longitude, M is the mean anomaly, ϖ is the longitude of pericenter, a is the semi-major axis,

momenta. As long as this is the case, we can write the Lagrangian $\mathcal{L} = K - V$, where K is the kinetic energy and V includes the fictitious potentials.

and e is the eccentricity, all appropriate to the KBO. Furthermore, $\mu \equiv Gm_\odot$. These variables are modified from the standard set of Poincaré variables in order to describe the motion of a massless test particle. The Hamiltonian reads

$$H = -\frac{\mu^2}{2\Lambda^2} - R(t). \quad (8)$$

The perturbation R is a function of $\lambda_N(t)$, which is explicitly time-dependent.

To eliminate the explicit time-dependence in R , we perform a point transformation. Inside the 2:1 resonance, it is illuminating to employ the following coordinates:

$$\phi = 2\lambda - \lambda_N(t) - \varpi, \quad \sigma = \lambda - \lambda_N(t), \quad (9)$$

for which the corresponding momenta equal

$$\Gamma, \quad N = \Lambda - 2\Gamma. \quad (10)$$

We are interested in the evolution of ϕ (see §2.1), and our choice for σ will allow us to average over the synodic period easily.

The new time-independent Hamiltonian reads

$$\begin{aligned} \tilde{H} &= H - n_N(\Gamma + N) \\ &= -\frac{\mu^2}{2(N + 2\Gamma)^2} - n_N(\Gamma + N) - R(\phi, \sigma, \Gamma, N), \end{aligned} \quad (11)$$

where n_N is the mean motion of Neptune. The price we pay in eliminating the explicit time-dependence is the appearance of an extra term in the Hamiltonian, $-n_N(\Gamma + N) = -n_N|\mathbf{r} \times \dot{\mathbf{r}}|$. This term renders \tilde{H} equivalent to the Jacobi constant. This formulation of the Hamiltonian will be useful when we allow Neptune to migrate in §3.

We are interested in the behavior of our system over timescales longer than the synodic period. We therefore average over the synodic period to obtain our final Hamiltonian. The averaged disturbing function equals

$$\begin{aligned} R_{\text{avg}} &= \frac{1}{2\pi} \int_0^{2\pi} R d\sigma \\ &= \frac{Gm_N}{2\pi} \int_0^{2\pi} \left(\frac{1}{|\mathbf{r} - \mathbf{r}_N|} - \frac{\mathbf{r}_N \cdot \mathbf{r}}{|\mathbf{r}_N|^3} \right) d\sigma. \end{aligned} \quad (12)$$

The total averaged Hamiltonian is

$$H_{\text{avg}} = -\frac{\mu^2}{2(N + 2\Gamma)^2} - n_N(\Gamma + N) - R_{\text{avg}}(\phi, \Gamma, N). \quad (13)$$

This Hamiltonian does not depend on σ . Therefore N is a constant of the motion: $\partial H_{\text{avg}}/\partial \sigma = -\dot{N} = 0$.

Figure 4 displays level curves of H_{avg} as well as individual contributions to H_{avg} from the direct and indirect terms. In Figures 4, 5, and 6, we set $m_N = 10^{-3}m_\odot$. Had we used Neptune's true mass ($m_N = 5.15 \times 10^{-5}m_\odot$), contours of symmetric and asymmetric libration would be less pronounced. When the planet is not migrating, the test particle's orbit evolves along a contour of constant Hamiltonian. The axes are $k = e \cos \phi$ and $h = e \sin \phi$, so that the distance from the center of each plot is the eccentricity and the azimuthal angle is ϕ . The semi-major axis and eccentricity of the test particle are related by

$$a = \frac{1}{\mu} \left(\frac{N}{2\sqrt{1 - e^2} - 1} \right)^2 \quad (14)$$

where $\alpha = a_N/a$ and the f_i 's are functions of Laplace coefficients given in Murray & Dermott (1999). We have dropped terms that average to zero over the synodic period. The Hamiltonian, expanded to second order and averaged over the synodic period, is

$$H_{\text{avg},2} = H_{\text{base}} - R_{\text{avg},2} . \quad (17)$$

This second-order expansion generates contours of asymmetric libration but no artificial islands in inappropriate locations; it provides a good qualitative representation of the actual potential. For example, the contours in the top left panel of Figure 4 and the top right panel of Figure 5 are qualitatively similar, though the stable points in the two plots have somewhat different values of ϕ .

Whereas Equation 16 suggests that asymmetric libration arises from the second-order term in a power-series expansion of the disturbing function, we emphasize that such a conclusion is misleading from a physical point of view. Asymmetric libration relies on a balance between the direct and indirect perturbations; it depends on the indirect term not time-averaging to zero. Expanding the direct term to infinite order while excluding the indirect term would not yield asymmetric libration. Beaugé (1994) illustrates the difficulty of attributing asymmetric libration to the second-order term by truncating the potential for the 3:2 resonance at second order and finding asymmetric libration where there should be none. Equation 16 should be regarded as simply a useful fitting formula for the true potential.

3. THE ORIGIN OF ASYMMETRIC CAPTURE

We now explain the origin of asymmetric capture when the planet is migrating. As the planet migrates outward, it may capture test particles that begin outside resonance into resonance [see, e.g., Murray & Dermott (1999), and references therein]. To be caught into asymmetric resonance from an initially circulating orbit, a test particle must first be caught into symmetric resonance. This may be seen qualitatively using a series of level diagrams for the Hamiltonian, and quantitatively by numerically integrating the equations of motion (§3.1). We recall from Goldreich (1965) that migration induces an offset in the stable point of symmetric libration (§3.2). We expand upon these two observations to explain the differing probabilities of capture into the two islands of asymmetric resonance. We elucidate three separate physical effects and provide a series of diagnostic numerical integrations (§3.3). We provide a sample prediction of the analytic theory (§3.4), and compare it with numerical experiments that solve for the ratio of particles captured into libration about the two islands as a function of migration timescale and other initial conditions (§3.5).

3.1. The Transition from Circulation to Asymmetric Libration

Before a test particle can be captured into asymmetric libration, it must first be captured into symmetric libration. To explain why this is so, we appeal to the contour plots discussed in §2.2. Consider the limit in which the timescale for migration is long compared to the libration period. Then, over timescales short compared to the migration time, the particle's orbit evolves approximately

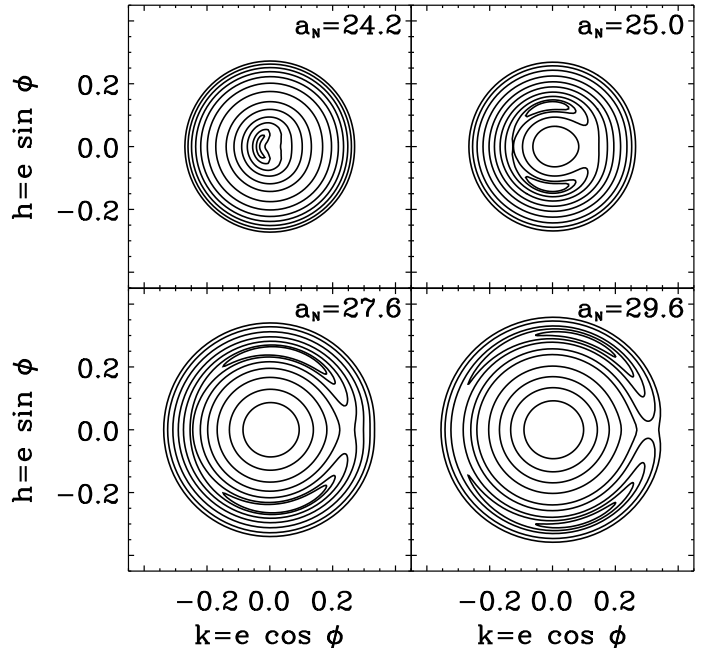


FIG. 6.— Sequence of level diagrams of H_{avg} for fixed $N = 6.2\sqrt{Gm_{\odot}} \text{ AU}^{1/2}$ and increasing a_N , marked on the plots in AU. Here, $m_N = 10^{-3}m_{\odot}$. A particle whose a is too large to be in resonance stays on approximately the same circulating contour at a large distance from the origin before resonance capture. As Neptune migrates outward, the resonance expands outward to encounter the particle.

along a contour of constant exact Hamiltonian, H_{avg} .⁷ Over timescales comparable to the migration time, we obtain a qualitative sense of the evolution of the particle's orbit by considering a progression of contour plots corresponding to different values of a_N . Such a progression is displayed in Figure 6, in which panels correspond to the same value of the adiabatic invariant, N , but increasing values of a_N . Even when Neptune is migrating, the Hamiltonian (averaged over the synodic period) is still given by H_{avg} ; while n_N and R_{avg} are now explicit functions of time, N is still a constant of the motion.

In the panels of Figure 6, a larger value for e corresponds to a larger value for a by conservation of N (Eqn. 14). As Neptune migrates outward, the libration centers migrate outward as well. A particle having too large an a to be in resonance circulates in the outer regions of the plots, maintaining approximately its same distance from the origin prior to resonance encounter. The resonance appears to approach such a particle, which will eventually find itself on a contour of symmetric libration. Since the asymmetric contours are all surrounded by symmetric contours and the evolution of the potential is smooth, a particle in asymmetric resonance must previously have occupied a symmetric contour.

We confirm the evolutionary sequence from circulation

⁷ Level diagrams in this paper are drawn for fixed values of a_N . Level diagrams showing the exact paths of particles in e - ϕ space when a_N varies with time cannot be made because then the potential is time-dependent.

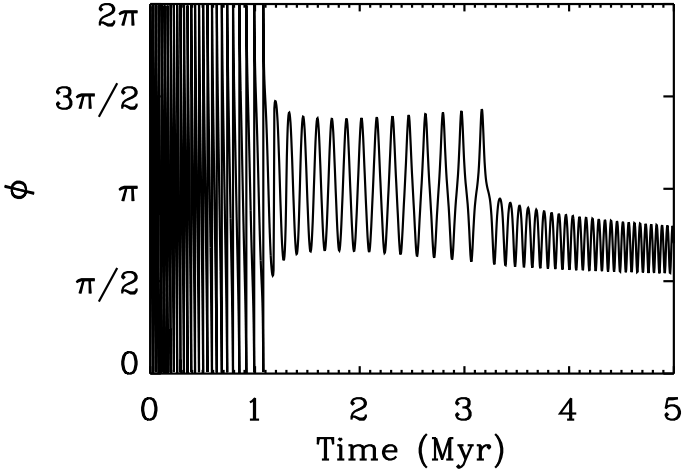


FIG. 7.— Evolution of ϕ from circulation to symmetric libration to asymmetric libration as the planet migrates outward. In this figure, m_N is set equal to Neptune’s true mass. The planet migrates according to Equation 19 with $t_0 = 300$ Myr and $a_{N,0} = 23.1$ AU. Time on the plot is measured from $t = 311$ Myr when the particle is characterized by $\phi = 0$, $e = 0.01$, and $a = 37.67$ AU (1 AU outside of nominal resonance).

to symmetric libration to asymmetric libration by numerically integrating the equations of motion for ϕ . We employ the expanded Hamiltonian, $H_{\text{avg},2}$. As discussed in §2.2.2, this expansion reproduces the asymmetric islands in the exact Hamiltonian qualitatively well. Our Hamiltonian equals

$$H_{\text{avg},2}(\phi, \Gamma, N, t) = -\frac{\mu^2}{2(N+2\Gamma)^2} - n_N(\Gamma + N) - \frac{Gm_N}{a_N} \left[\alpha(f_1 + f_2 e^2 + f_{31} e \cos \phi + f_{53} e^2 \cos 2\phi) - \frac{1}{2\alpha} e \cos \phi \right] \quad (18)$$

where $e = e(\Gamma, N)$. We prescribe

$$a_N = a_{N,0} \left(\frac{t}{t_0} \right)^{2/3}, \quad (19)$$

where $a_{N,0}$ and t_0 are constants, so that $\alpha = \alpha(\Gamma, N, t)$ and $n_N = n_N(t)$. The f ’s are held constant in our computations. The form of this prescription for Neptune’s migration will be motivated in the next section.

The equations of motion,

$$\dot{\phi} = \frac{\partial H_{\text{avg},2}}{\partial \Gamma}, \quad \dot{\Gamma} = -\frac{\partial H_{\text{avg},2}}{\partial \phi}, \quad (20)$$

are integrated using the Bulirsch-Stoer algorithm (Press et al. 1992). A sample time evolution for ϕ is showcased in Figure 7, with input parameters listed in the caption. The particle initially circulates, then librates symmetrically, and finally is captured into asymmetric libration.

3.2. Migration-Induced Offset in Symmetric Libration

A key ingredient in understanding asymmetric capture is the fact that for symmetric libration, planetary migration induces an offset, $\Delta\phi$, in the libration center, so that

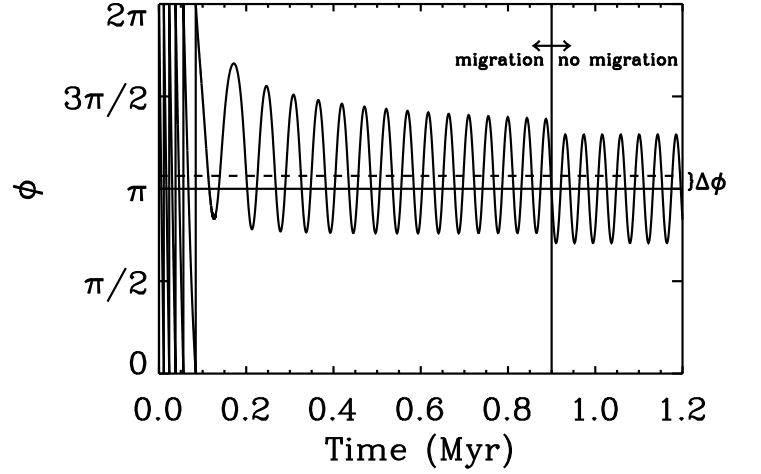


FIG. 8.— Migration-induced offset in the stable point of symmetric libration. Over the first 0.9 Myr shown, the planet migrates; over the remainder of the plot, the planet’s orbit is fixed. The dashed line indicates the offset due to migration, $\Delta\phi$, calculated using Equation 26 at the plotted time of 0.6 Myr; the agreement with the numerical integration is excellent. For this integration, we drop the term proportional to $\cos(2\phi)$ in $R_{\text{avg},2}$ and set m_N equal to the mass of Neptune. The planet migrates according to Equation 19, with $t_0 = 10$ Myr and $a_{N,0} = 23.1$ AU. Time on the plot is measured from $t = 10.3$ Myr when the particle is characterized by $\phi = 0$, $e = 0.04$, and $a = 37.67$ AU (1 AU outside of nominal resonance).

the stable point lies at $\phi = \pi + \Delta\phi$. Goldreich (1965) finds that to first order in the eccentricity of the particle, symmetric libration is described by the formula

$$\frac{d^2(\delta\phi)}{dt^2} = -\gamma^2 \delta\phi - \frac{dn_N}{dt}, \quad (21)$$

where $\delta\phi = \phi - \pi$ is small, and $2\pi/\gamma$ is the libration period. The term $-dn_N/dt$ arises from migration; since $\phi = 2\lambda - \lambda_N - \varpi$, $\dot{\phi}$ due to migration equals $-\dot{\lambda}_N = -\dot{n}_N$. Equation 21 integrates to

$$\delta\phi = \theta \sin \gamma t - \frac{1}{\gamma^2} \frac{dn_N}{dt}, \quad (22)$$

where θ is the amplitude of libration. Equation 22 describes libration of ϕ about $\pi + \Delta\phi$, where the angular offset

$$\Delta\phi = -\frac{1}{\gamma^2} \frac{dn_N}{dt}. \quad (23)$$

When Neptune migrates outward, $\Delta\phi$ is positive. The magnitude of the offset is

$$\Delta\phi = \frac{3}{4\pi} \frac{T_1^2}{T_m T_o}, \quad (24)$$

where T_1 is the libration period, $T_m = a_N/\dot{a}_N$ is the migration timescale, and T_o is Neptune’s orbital period. The libration timescale equals

$$T_1 \approx C T_o \sqrt{\frac{m_\odot}{m_N}} e^{-1/2}, \quad (25)$$

where $C(\alpha) = 1/\sqrt{6\alpha^3[2f_{31}(\alpha) - \alpha^{-2}]} \approx 0.9$. Combining these expressions, we find that the offset angle is

$$\Delta\phi \approx \frac{3C^2}{4\pi} \frac{T_o}{T_m} \frac{m_\odot}{m_N} \frac{1}{e}. \quad (26)$$

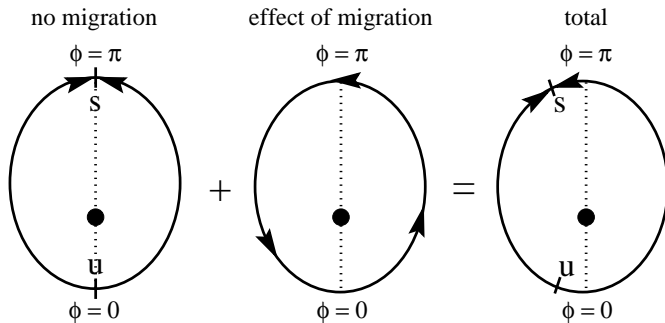


FIG. 9.— Schematic of the accelerations of ϕ for symmetric libration. The letters ‘s’ and ‘u’ mark stable and unstable equilibria, respectively. When Neptune is not migrating, ϕ accelerates toward π (left). Neptune’s migration accelerates ϕ toward larger values (center). These contributions combine to yield acceleration toward a stable point greater than π , and acceleration away from an unstable point less than 2π (right).

In Equations 25 and 26, e should be evaluated at exact resonance.

We can verify this offset numerically. The Hamiltonian given in Equation 13 with R_{avg} expanded to first order in e reproduces symmetric libration qualitatively correctly (§2.2.2). We integrate the equations of motion for this Hamiltonian, again forcing Neptune to migrate according to Equation 19.⁸ By inserting Equation 19 into Equation 26, we see that our prescription for migration yields an offset, $\Delta\phi$, that is approximately constant with time, modulo the effect of the changing eccentricity of the KBO. Figure 8 displays a sample time evolution for ϕ and verifies that this is the case. The center of symmetric libration is shifted above π by an amount, $\Delta\phi$, that agrees with Equation 26. The input parameters for the integration are supplied in the caption to Figure 8.

Physically, the offset occurs because as a_N increases, the planet’s angular speed decreases. Each conjunction occurs later than it would in the absence of migration; migration accelerates ϕ toward larger values. As a result, the stable point of ϕ increases; see Figure 9 for a schematic description. The offset is akin to the shift in the equilibrium position of a spring in the presence of a constant gravitational field.

The stable points of asymmetric libration are also shifted forward by outward migration. Figure 10 displays integrations, using $H_{\text{avg},2}$, for which the migration is turned off after capture into asymmetric resonance. The libration centers in the absence of migration relax to smaller values of ϕ . Figure 11, analogous to Figure 9, explains the shifts pictorially.

3.3. Deciding Between the Two Libration Centers

Keeping in mind that all libration centers—both for symmetric and asymmetric resonance—shift due to Neptune’s migration, we now turn to the question of which island of asymmetric libration captures a greater proportion of particles. We will refer to the asymmetric libration center with $\phi < \pi$ as the “leading” center and to the center with $\phi > \pi$ as the “trailing” center. We choose this terminology because in a snapshot of an ensemble

⁸ For this integration, we drop only the term proportional to $\cos(2\phi)$ from Equation 16; this permits ease of comparison with later integrations in which we restore this term.

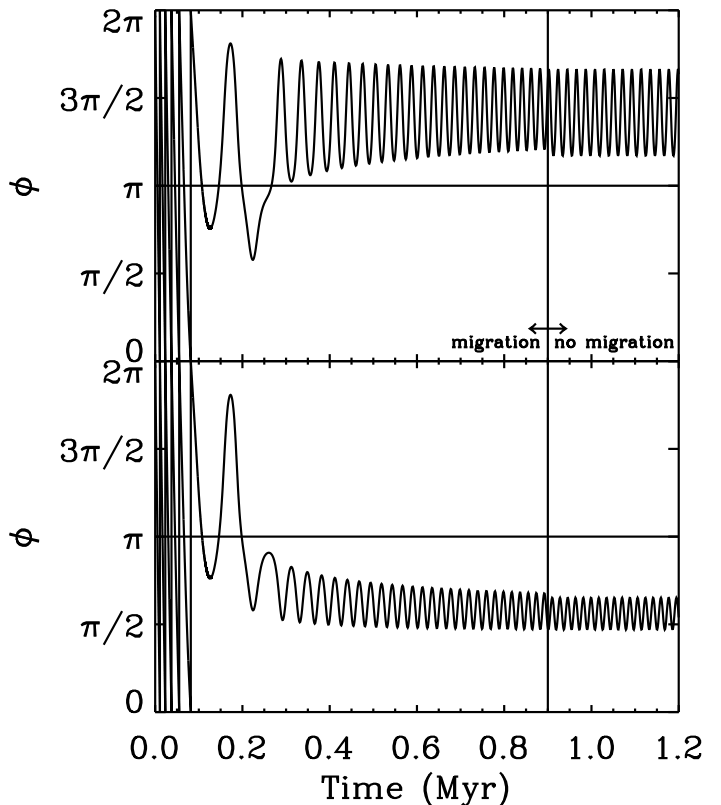


FIG. 10.— Migration-induced offsets in asymmetric libration. Two evolutions of ϕ exhibiting asymmetric libration are shown, one ending in the trailing island ($\phi > \pi$, top), and the other ending in the leading island ($\phi < \pi$, bottom). The planet migrates from time 0 to 0.9 Myr and subsequently its orbit is fixed. Both centers of asymmetric libration are shifted to larger values during the migration. The migration parameters are the same as those in Figure 8 except that here, R_{avg} is expanded to second order in e and at the plotted time of 0, $\phi_0 = 6.19$ (top) and 6.22 (bottom).

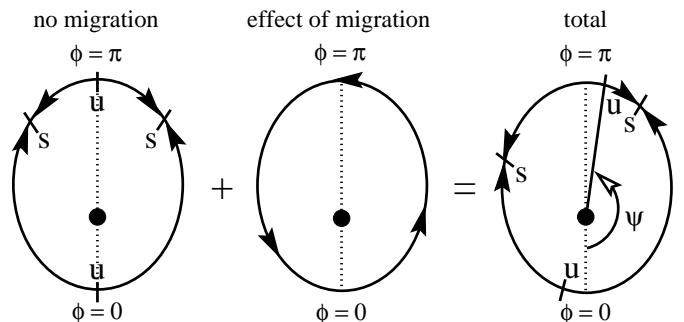


FIG. 11.— Schematic of the accelerations of ϕ for asymmetric libration. The letters ‘s’ and ‘u’ mark stable and unstable equilibria, respectively. When Neptune is not migrating, ϕ accelerates toward the two stable points (left). Neptune’s migration accelerates ϕ toward larger values (center). These effects combine to shift the two stable points to larger ϕ and the two unstable points to smaller ϕ (right). The angle $\psi < \pi$ marks the location of one of the shifted unstable equilibrium points. Note how the stable and unstable points are squeezed together at $\phi < \pi$.

of resonant particles (see CJ), particles librating about the leading center ($\phi < \pi$) both attain perihelion and spend a greater fraction of the synodic period at longitudes greater than that of Neptune (see Figure 3). As a consequence, these particles appear to cluster at longitudes greater than that of Neptune. Conversely, particles librating about the trailing center ($\phi > \pi$) cluster at longitudes less than that of Neptune.

We identify three separate factors that determine the relative capture probabilities.

3.3.1. Migration-Induced Offsets Favor Trailing Island

If, as a particle transitions from symmetric to asymmetric libration, ϕ is greater than some angle ψ , then the particle is caught into the trailing island, while if $\phi < \psi$, the particle is caught into the leading island. At first glance, one might expect that $\psi = \pi$, but in fact $\psi < \pi$. Figure 11 illustrates how the addition of the acceleration of ϕ due to migration, $\ddot{\phi} = -\dot{n}_N > 0$, shifts the two stable equilibria to larger ϕ and the unstable equilibria to smaller ϕ . The unstable equilibrium point that was located at $\phi = \pi$ in the absence of migration is shifted by migration to a value $\psi < \pi$.

To estimate ψ analytically, we perform calculations that are analogous to those that yield Equation 21 and that incorporate the second-order resonant term in the disturbing function. For small $\delta\phi = \phi - \pi$,

$$\frac{d^2(\delta\phi)}{dt^2} \approx -A\gamma^2\delta\phi - \frac{dn_N}{dt}, \quad (27)$$

where $A(\alpha, e) = 1 - 8ef_{53}(\alpha)/[2f_{31}(\alpha) - \alpha^{-2}] \approx 1 - 34e$. For $A > 0$, symmetric libration occurs with frequency $A^{1/2}\gamma$ and asymmetric libration is forbidden. The impossibility of asymmetric libration for $e \lesssim 0.03$ ($A \gtrsim 0$) is not an artifact of our second-order expansion of the Hamiltonian. It is true even under the exact Hamiltonian, as can be seen by careful examination of level diagrams of the Hamiltonian.

For $A < 0$, asymmetric libration becomes possible; the unstable equilibrium point, located at $\phi = \pi$ in the absence of migration, is shifted by migration to

$$\psi \approx \pi + A^{-1}\Delta\phi < \pi, \quad (28)$$

where $\Delta\phi$ is given by Equation 23. The coefficient $A^{-1} \approx -2.8$ for $e = 0.04$.

The relative likelihoods of capture into the two islands depend on the time spent in symmetric resonance librating at $\phi > \psi$ and $\phi < \psi$. Migration shifts the unstable equilibrium point dividing the two islands backward by $A^{-1}\Delta\phi$. Migration also shifts the center of symmetric libration forward by $\Delta\phi$. These two effects compound to render capture into the trailing island more likely.

We can verify numerically the value of the transition angle, ψ . Figure 12 displays two evolutions of ϕ that start with slightly different initial values for ϕ . The solid horizontal line marks $\phi = \pi$, and the dashed line marks $\phi = \psi$, evaluated using Equation 28 near the time at which the particle trajectories appear to diverge. The particle that transitions from symmetric to asymmetric resonance when $\phi < \psi < \pi$ is caught into the leading island, while the particle that makes the transition when $\phi > \psi$ is caught into the trailing island. To the extent that particles in symmetric libration spend more time

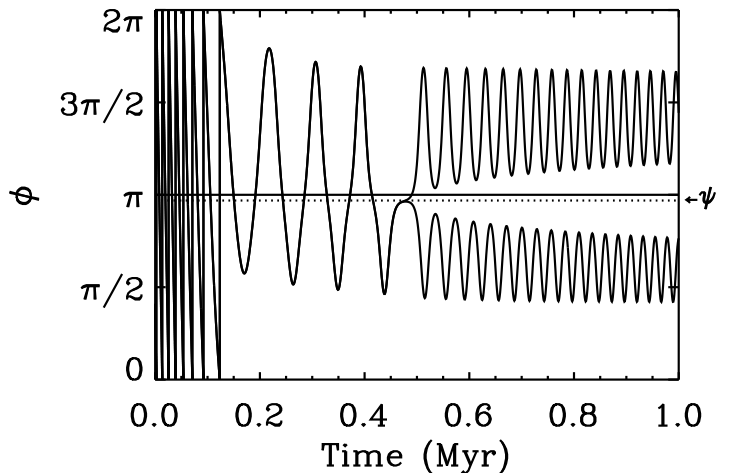


FIG. 12.— Migration-induced offset in the unstable point dividing the two islands of asymmetric resonance. Shown are two evolutions of ϕ with slightly different initial values of ϕ . The solid horizontal line marks $\phi = \pi$, and the dotted line marks $\phi = \psi$, evaluated according to Equation 28 at the plotted time of 0.48 Myr. If $\phi > \psi$ at the moment the particle transitions from symmetric to asymmetric resonance, then the particle is caught into the trailing island ($\phi > \pi$); if $\phi < \psi$, then the particle is caught into the leading island ($\phi < \pi$). The location of the dividing angle inferred from these integrations is well predicted by Equation 28. Note also how the symmetric librations near the plotted time of ~ 0.3 Myr are shifted above $\phi = \pi$; this is the same effect documented in Figures 8 and 9 and §3.2. For this integration, m_N is set equal to the mass of Neptune. The planet migrates according to Equation 19, with $t_0 = 15$ Myr and $a_{N,0} = 23.1$ AU. Time on the plot is measured from $t = 15.45$ Myr when the particles are characterized by $\phi = 1.2873$ and 1.2876 , $e = 0.04$, and $a = 37.67$ AU (1 AU outside of nominal resonance).

with $\phi > \psi$ than with $\phi < \psi$ —and note how the symmetric librations are shifted above $\phi = \pi > \psi$ —we expect more particles to be captured into the trailing island. Further quantitative analysis is supplied in §3.4.

3.3.2. Libration Amplitude in Symmetric Resonance and Dependence on Initial Eccentricity

The amplitude of libration exhibited by a particle in symmetric resonance depends on the particle's eccentricity prior to resonance capture, with larger initial eccentricities producing larger libration amplitudes. Larger libration amplitudes in symmetric resonance imply that the migration-induced offsets described in §3.2 and §3.3.1 are less effective at changing the ratio of the times spent at $\phi < \psi$ and $\phi > \psi$. We therefore expect the capture probabilities between the two islands to equalize with larger initial eccentricities. Figure 13 illustrates the effect. Note that larger eccentricities not only produce larger amplitudes of libration, but also reduce the magnitudes of the offsets $\Delta\phi$ and $\pi - \psi$, as is evident from Equations 26 and 28 (the latter for $e \gtrsim 0.03$).

3.3.3. Uneven Libration Rates and Reversal of Capture Asymmetry

We have argued that the ratio of particles captured into the trailing and leading islands is determined by the ratio of times a particle spends with $\phi > \psi$ and

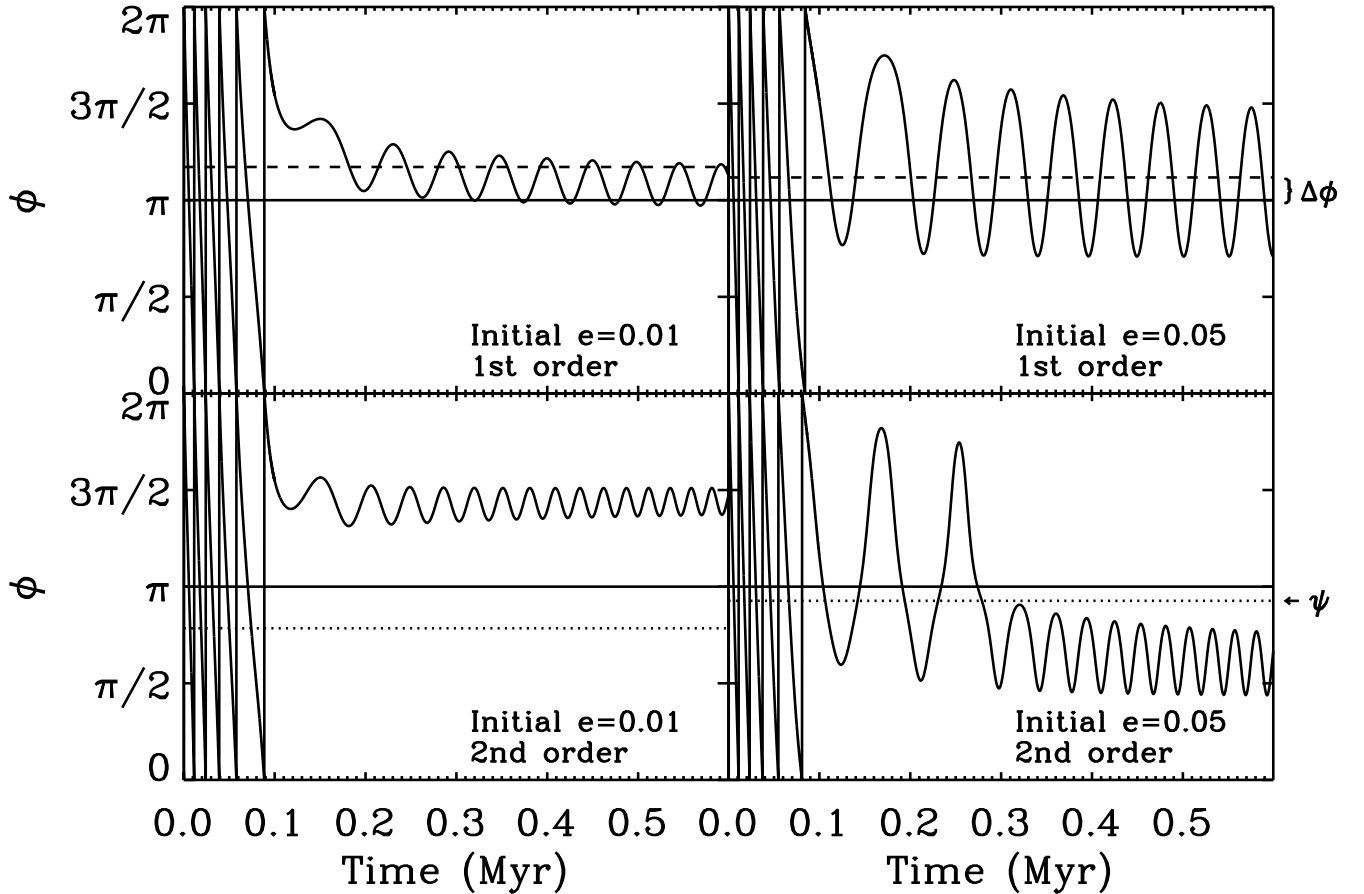


FIG. 13.— Effect of initial eccentricity on the evolution of ϕ . Smaller initial eccentricities yield smaller amplitudes of libration and greater likelihoods of capture into the trailing island ($\phi > \pi$). Initial eccentricities equal 0.01 in the left two panels and 0.05 in the right two panels. In the top two panels, ϕ evolves under the potential in which the term proportional to $\cos(2\phi)$ is dropped, yielding symmetric libration. The dashed lines indicate the value of $\pi + \Delta\phi$ evaluated using Equation 26 at the plotted time of 0.2 Myr. In the bottom two panels, the potential is expanded to second order in e , yielding the possibility of asymmetric libration. The dotted lines indicate the value of ψ calculated using Equation 28 at a time of 0.2 Myr. Solid horizontal lines mark $\phi = \pi$. Remaining initial conditions are the same for all four panels: the planet has the mass of Neptune and migrates according to Equation 19, with $t_0 = 10$ Myr and $a_{N,0} = 23.1$ AU. Time on the plots is measured from $t = 10.3$ Myr when the particles are at $\phi = 0.126$ and $a = 37.67$ AU (1 AU outside of nominal resonance).

with $\phi < \psi$ while in symmetric libration. These times are determined not only by the range of values spanned by ϕ during symmetric libration, but also by the rate at which the particles librate, i.e., $\dot{\phi}$ as a function of ϕ . Immediately before the transition from symmetric to asymmetric libration, a particle librates more slowly when $\phi < \psi$ than when $\phi > \psi$, opposing the tendency to spend more time at $\phi > \psi$ as described in §3.3.1. Surprisingly, this effect can be large enough to favor the leading island for some initial conditions and to reverse the usual sense of the capture asymmetry.

Figure 14 provides a series of snapshots of an ensemble of particles beginning in circulation and ending in asymmetric resonance. For this integration, we use the more realistic migration prescription,

$$a_N(t) = a_{N,f} - (a_{N,f} - a_{N,0})e^{-t/\tau}, \quad (29)$$

where $a_{N,0} = 23.1$ AU is Neptune's initial semi-major axis, $a_{N,f} = 30.1$ AU is Neptune's final semi-major axis, and τ is a time constant. In circulation (curve 1), parti-

cles are evenly distributed over an approximate circle, reflecting the rough constancy of $\dot{\phi}$. In symmetric libration (curve 2), ϕ changes more slowly near the turning points of the libration. This slowing is evident as a clumping of particles near extrema of ϕ .

Immediately preceding the transition from symmetric to asymmetric resonance (Figure 14, curve 3), the level curve of symmetric libration deforms to just surround the islands of asymmetric libration into which the particles will eventually be caught. The leading island is smaller than the trailing island due to migration-induced offsets in the stable and unstable equilibria (see Figure 11). Despite the smaller size of the leading island, however, particles still tend to clump in its vicinity, reflecting smaller values of $\dot{\phi}$ there than near the trailing island. The result, after the last contour of symmetric libration finally fissions (curve 4), is a tendency to capture more particles into the leading island.

The greater degree of slowing near the leading island may be crudely understood by noting that at $\phi < \psi$, the

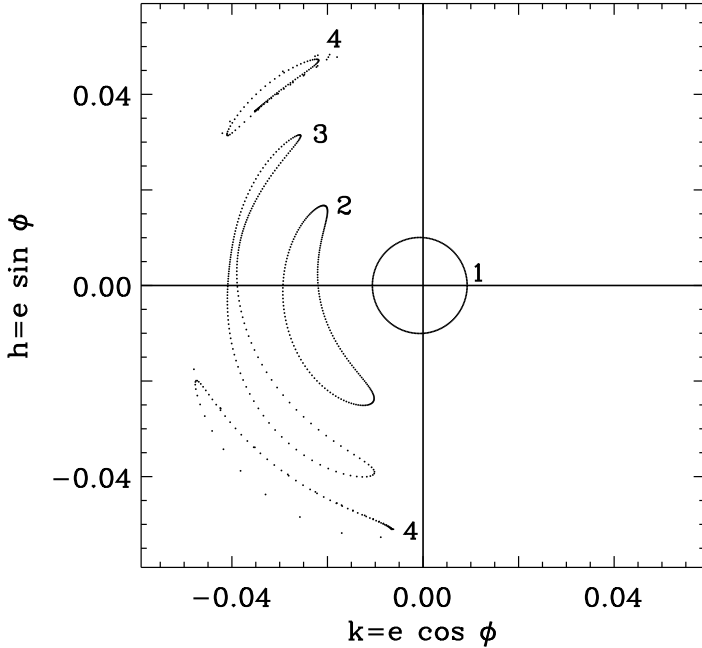


FIG. 14.— Evolution from circulation (curve 1) to symmetric libration (curves 2 and 3) to asymmetric libration (curve 4) of a collection of 200 particles that initially share the same value of the Hamiltonian. Each point represents the phase space position of a single particle recorded at 1 of 4 instants. Neptune migrates according to Equation 29, with $\tau = 45$ Myr. Snapshots are taken at times $t = 2.75$ Myr (curve 1), 4.40 Myr (curve 2), 4.73 Myr (curve 3), and 5.10 Myr (curve 4). At $t = 0$, $e \approx 0.01$ and $a \approx 37.67$ AU (1 AU outside of nominal resonance) for each particle. (Since level curves of the Hamiltonian are not exact circles even in circulation, initial eccentricities and semi-major axes of particles on a level curve are slightly different.) Note, in curve 3, the tendency of particles to cluster at $\phi < \pi$, despite the greater range of values accessible at $\phi > \pi$.

unstable and stable points are closely juxtaposed (Figure 11). Since both points correspond to $\dot{\phi} = 0$, the potential in this region of phase space should be relatively flat. Particles having small $\dot{\phi}$ near this turning point of symmetric libration spend a comparatively long time traversing a nearly flat potential.

3.4. A Sample Quantitative Estimate

We use our analytic model to estimate the minimum migration speed above which capture into the trailing island is overwhelmingly preferred over capture into the leading island. Capture into the leading island is impossible if, at the time of transition from symmetric to asymmetric resonance, the libration angle ϕ fails to attain values less than ψ , i.e., if the sum of both migration-induced offsets is greater than the amplitude of symmetric libration:

$$\Delta\phi + (\pi - \psi) \gtrsim \theta. \quad (30)$$

All quantities in this expression should be evaluated at the time of capture into asymmetric resonance. Using Equations 26 and 28, we re-write the above criterion as

$$T_m \lesssim (1 - A^{-1}) \frac{3C^2 m_\odot T_o}{4\pi m_N e\theta}. \quad (31)$$

We may estimate θ as a function of e in the adiabatic limit. In this limit, at the time of transition into asymmetric libration, the contour of constant Hamiltonian on which the particle lies (the “asymmetric separatrix”) contains an unstable point at $\phi = \pi$. On the asymmetric separatrix, the turning points of libration have approximately the same value of e as the value at $\phi = \pi$. Then Equation 18 requires that

$$\alpha(f_{31}e \cos \phi_{\text{tp}} + f_{53}e^2 \cos 2\phi_{\text{tp}}) - \frac{1}{2\alpha}e \cos \phi_{\text{tp}} \approx \alpha(f_{31}e \cos \pi + f_{53}e^2 \cos 2\pi) - \frac{1}{2\alpha}e \cos \pi \quad (32)$$

where ϕ_{tp} gives the values of ϕ at the turning points:

$$\phi_{\text{tp}} = \cos^{-1} \left[1 - \frac{B(\alpha)}{e} \right] \quad (33)$$

and $B(\alpha) \equiv [\alpha f_{31} - 1/(2\alpha)]/[2\alpha f_{53}] \approx 0.058$. The amplitude of libration is

$$\theta(e) = |\pi - \phi_{\text{tp}}(e)|. \quad (34)$$

For $m_N/m_\odot = 5 \times 10^{-5}$ and $a_0 = 37.67$ AU, the integration displayed in Figure 14 offers the value $e \approx 0.04$ at the time of transition from symmetric to asymmetric resonance. Equation 34 then yields $\theta \approx 1.1$, consistent with the amplitude shown in Figure 14. From these values, we calculate that the critical value of T_m below which capture into the trailing island is overwhelmingly preferred is $T_{m,\text{crit}} \sim 3.8 \times 10^7$ yr. In the next section on numerical integrations, we check the accuracy of this estimate.

The only remaining parameter for which we have yet to supply an analytic expression is the eccentricity at the transition from symmetric to asymmetric libration. To estimate this, one could work again in the adiabatic limit, using the adiabatic invariant, $J \equiv \oint \Gamma d\phi$ (approximately proportional to the area enclosed by the path of a particle in h - k space in the small e limit). The value of J in symmetric libration equals the value of J appropriate to the asymmetric separatrix that the particle crosses. One could exploit this fact to identify that separatrix and its associated value of e . Another improvement would be to compute the relative times that ϕ spends above and below ψ when Equation 30 is not satisfied. Such a calculation would have to account for the anharmonicity of motion in asymmetric libration (see, e.g., Malhotra 1996), an anharmonicity that is only accentuated when the perturber migrates (see §3.3.3).

We do not pursue these additional computations analytically, but rather content ourselves with our physical, order-of-magnitude understanding of asymmetric capture embodied in Equations 31–34 and proceed with more numerical explorations in the next section. We note in passing that the resonance capture theory of Henrard (1982) and the analytic estimates of capture probabilities derived therefrom (Borderies & Goldreich 1984) cannot be applied to the problem of asymmetric capture without substantial modification. This is because such theories are written in the strict adiabatic limit in which the migration timescale is infinitely longer than the libration timescale. But asymmetric capture relies upon a finite migration timescale. In other words, migration-induced offsets are absent from the theory of Henrard (1982).

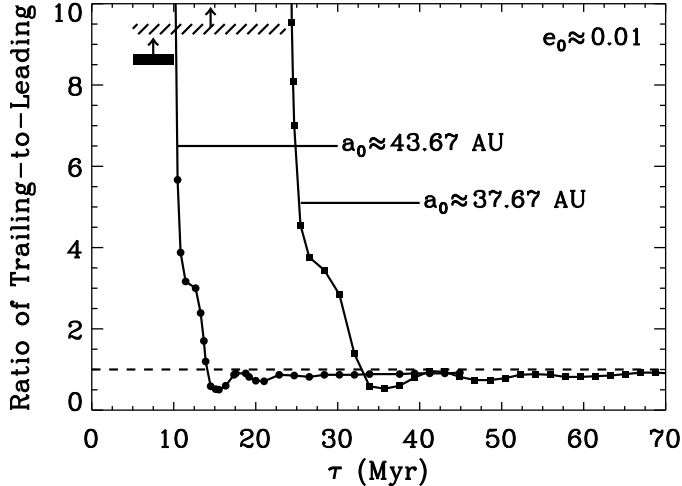


FIG. 15.— Dependence on the exponential migration timescale, τ , of the ratio of particles captured into trailing vs. leading asymmetric resonance assuming low initial eccentricities ($e_0 \approx 0.01$). Horizontal (solid and hatched) bars correspond to a ratio of ∞ . For fast migration, more particles are caught into the trailing island, and for slow migration, the ratio is near 1. For all timescales with a ratio plotted, 100% of particles are captured from circulation. For this plot, the mass of the planet is Neptune’s true mass, and Neptune migrates according to Equation 29, with $a_{N,0} = 23.1$ AU and $a_{N,f} = 30.1$ AU. Each ratio is calculated by following 200 particles that initially circulate, have the same Hamiltonian value, and are spaced evenly in ϕ_0 . The hatched bar corresponds to particles having initial semi-major axes of $a_0 \approx 37.67$ AU (1 AU outside of nominal resonance), and the solid bar corresponds to $a_0 \approx 43.67$ AU (7 AU outside of nominal resonance). Because Neptune’s migration rate decreases exponentially with time, Neptune is migrating more slowly when it captures particles that start further from resonance. As a result, particles having $a_0 \approx 37.67$ AU are asymmetrically captured over a greater range of migration timescales as compared to those having $a_0 \approx 43.67$ AU.

3.5. Population Ratios as a Function of Migration Speed and Initial Eccentricity

We calculate numerically the ratio of captures into the trailing and leading islands as a function of migration timescale, initial semi-major axis, and initial eccentricity, using the migration prescription given by Equation 29. For a given τ , a set of η initial values of (a_0, e_0, ϕ_0) are computed which correspond to the same values of $H_{\text{avg},2}$ and N . If particles do not all start on the same Hamiltonian level curve, phase differences accumulate between particles and complicate interpretation of the final capture ratio. Initial values of a_0 and e_0 are chosen such that all particles begin in circulation; initial values of ϕ_0 are distributed uniformly from 0 to 2π . To achieve sufficient statistics, we select $\eta = 200$ or 800 depending on the efficiency of capture from circulation. Figure 15 plots capture ratios for particles with small initial eccentricity ($e_0 \approx 0.01$), while Figure 16 (top) supplies results for larger initial eccentricity ($e_0 \approx 0.05$). In each figure, two curves for two different values of a_0 are delineated, one starting approximately 1 AU away from resonance, and the other starting 7 AU away.

All three effects documented in §3.3 manifest themselves in Figures 15 and 16 (top). Shorter migration timescales yield greater asymmetries in the capture ra-

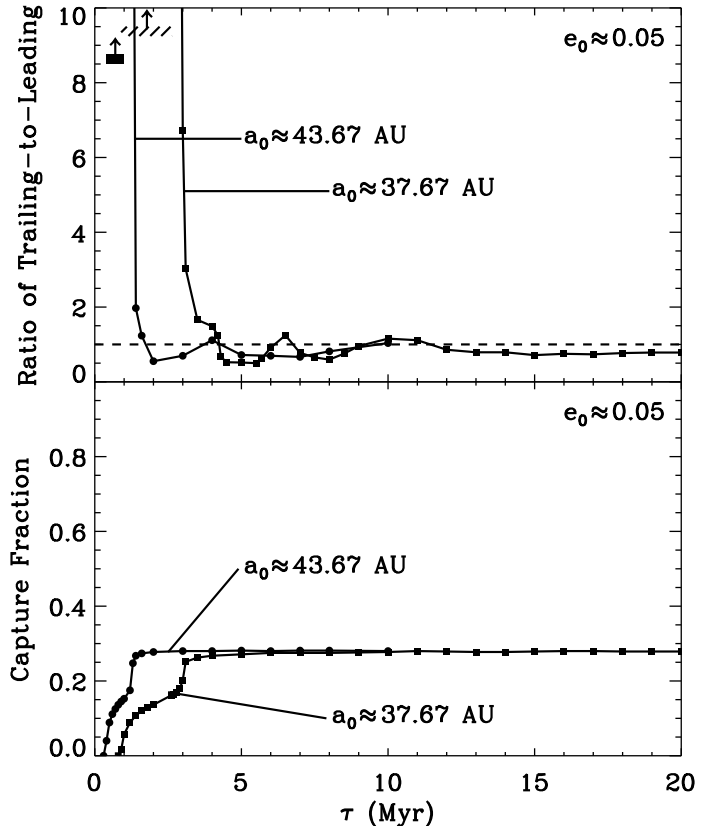


FIG. 16.— (Top) Dependence on the exponential migration timescale, τ , of the ratio of particles captured into trailing vs. leading asymmetric resonance assuming high initial eccentricities ($e_0 \approx 0.05$). Horizontal bars correspond to a ratio of ∞ . Fast migration yields large asymmetries favoring the trailing island, while slow migration yields ratios near 1. The timescale dividing these behaviors is shorter for $e_0 \approx 0.05$ than for $e_0 \approx 0.01$ (Figure 15); see §3.3.2 for an explanation. (Bottom) Fraction of particles caught from circulation. Note that large asymmetric capture ratios correspond to timescales shorter than those producing adiabatic capture fractions. Migration parameters are the same as those for Figure 15. Each datum is calculated by following 800 particles that initially circulate, have the same Hamiltonian value, and are spaced evenly in ϕ_0 . For the hatched bar, $a_0 \approx 37.67$ AU, and for the solid bar, $a_0 \approx 43.67$ AU. Neptune is migrating more slowly when it captures particles that start further from resonance.

tios, with preference given to capture into the trailing island, because of migration-induced offsets in the stable and unstable points of symmetric and asymmetric resonance (§3.3.1). For $e_0 \approx 0.01$, $\tau \lesssim 10$ Myr, and our chosen a_0 ’s, the probability of capture into the trailing island is overwhelming. Particles that originate from smaller semi-major axes are more likely to exhibit asymmetric capture because they are caught at earlier times when Neptune is assumed to have migrated more quickly. At large τ , the capture ratio approaches unity from below, a reflection of the nearly flat potential at $\phi < \psi$ (§3.3.3). The ratio of trailing-to-leading particles never dips below 0.5.

Our expectation, based on a simple calculation in §3.4, that the capture ratio is infinite if $T_m \equiv a_N/\dot{a}_N \lesssim 38$ Myr is largely borne out in Figure 15. The relevant curve is the one for $a_0 \approx 37.67$ AU, for which parameter values

best match those assumed for our calculation. The capture ratio is infinite for $\tau \lesssim 23$ Myr, which translates to $T_m = \tau a_N(t)/[a_{N,f} - a_N(t)] < 87$ Myr, a critical timescale that differs by a factor of 2.3 from our estimate in §3.4. The discrepancy could arise from our use of Equation 34, which is only correct in the adiabatic limit and for eccentricities that are not small, and our use of Equation 25, which is only correct in the limit of small libration amplitude.

As initial eccentricities of particles increase, capture into symmetric resonance becomes no longer certain.⁹ For $e_0 \approx 0.05$, the fraction of captured objects saturates at 28% for $\tau > 5$ Myr and decreases with shorter τ (Figure 16, bottom). Of those that are captured, strong asymmetries in the trailing-to-leading ratios do not appear except at $\tau \sim 1$ Myr because the larger amplitudes of symmetric libration caused by the larger initial (free) eccentricities weaken the effects of migration-induced shifts (§3.3.2). Moreover, the shifts themselves are smaller because of the larger eccentricities. For example, for $\tau = 10$ Myr and $e_0 \approx 0.01$, the ratio of trailing-to-leading particles can be infinite, while for the same τ and $e_0 \approx 0.05$, the ratio is near unity. The curves for $e_0 \approx 0.05$ are shifted to lower τ 's compared to those for $e_0 \approx 0.01$ by a factor of ~ 8 .

The computations we have just described and numerical simulations by CJ agree that the characteristic migration timescales required to produce strong asymmetric capture are in the range 10^6 – 10^7 yr. Equation 31 also suggests the same critical timescales. Our calculations yield larger asymmetries, however, than the purely numerical ones of CJ. For example, Figures 15 and 16 indicate that at $\tau = 10^6$ yr, the capture ratio is infinite, while CJ report a ratio of 3-to-1. We are unsure as to why there are differences, but the computations are at heart different: one employs a truncated version of the Hamiltonian and time-averages over the synodic period, while the other has no such approximations. While the semi-analytic model has served us well in illuminating the numerous physical effects underlying what was once a purely numerical result, we should probably rely on the numerical simulations for actual comparisons between theory and observation.

4. COMPARISON WITH OBSERVATIONS

Do the observations indicate symmetry or asymmetry in the distribution of 2:1 resonant KBOs with respect to the Sun-Neptune line? The Deep Ecliptic Survey (Chiang et al. 2003ab; Buie et al. 2003; Elliot et al. 2004) has developed a classification scheme that identifies resonant KBOs by virtue of their librating angles; an object is deemed resonant if three orbital integrations, each lasting 30 Myr and starting with initial conditions lying within the 3σ confidence surface of possible osculating orbits, all yield libration of the same resonance angle. By this criterion, 11 2:1 resonant KBOs (“Twotinos”) are identified, of which 2 librate symmetrically and 9 librate asymmetrically. Of the asymmetric librators, 2 librate about $\phi > \pi$ (trailing island), and 7 librate about $\phi < \pi$ (leading island). The current positions of all 11

Twotinos are displayed in Figure 17; they are overlaid on theoretical snapshots of Twotinos taken from CJ.

The observed asymmetry—2-to-7, in favor of the leading island—argues against a rapid migration history for Neptune. Given the initial conditions assumed by CJ—most notably initial eccentricities ranging uniformly from 0 to 0.05—the hypothesis that Neptune’s migration timescale was as short as $a_N/\dot{a}_N \sim 10^6$ yr predicts that the probability that a particle caught into asymmetric resonance is in the trailing island is $u \approx 0.75$ (CJ), with shorter migration timescales presumably giving rise to greater values of u . Given the observed (possibly biased—see below) asymmetry of 2-to-7, the probability that $u \geq 0.75$ ($\tau \leq 10^6$ yr) is 0.04%, where we have used the differential probability distribution $dP/du = (S+1)S!/[Y!(S-Y)!]u^Y(1-u)^{S-Y}$ (Port 1994, pages 264–265).¹⁰ Here $S = 9$ is the sample size and $Y = 2$ is the number of observed trailing objects. Thus, $\tau \leq 10^6$ yr seems unlikely. The probability that $u \geq 0.5$ ($\tau \leq 10^7$) is 5.5%.

4.1. Theoretical Caveats

One theoretical caveat to the above interpretation is that the capture probabilities into the two islands are sensitive to the particles’ initial eccentricities (see §3.3.2 and §3.5). The distribution of eccentricities assumed by CJ might not be realistic; see, e.g., Chiang et al. (2003ab) who present evidence that a fraction of the Kuiper belt was pre-heated to large eccentricities prior to resonance sweeping. If Twotinos today originated from larger eccentricity orbits prior to resonance capture, then migration timescales as short as $\sim 10^6$ yr would yield capture ratios closer to unity. However, objects on initially larger eccentricity orbits are less likely to be caught at all by the 2:1 resonance.

If we assume that Twotinos originated from circulating orbits having initial eccentricities $\lesssim 0.05$, then slow migration, on timescales longer than $\sim 10^7$ yr, is a more viable conclusion. Based on our computations, slow migration yields $0.33 \leq u \leq 0.5$. Given the observed asymmetry of 2-to-7, the probability that $0.33 \leq u \leq 0.5$ ($\tau \geq 10^7$ yr) is 24%.

A second theoretical caveat is the possibility that objects originally caught into one island transition to the other over the age of the solar system (Hahn, personal communication). We expect such mixing to afflict only objects having the largest libration amplitudes. Mixing has been reported by CJ on timescales as short as 10^7 yr for objects having libration amplitudes of 45° (see their figure 8). The Twotinos reported by the Deep Ecliptic Survey do not exhibit mixing on timescales as long as 30 Myr, but longer-term integrations have yet to be performed. A third caveat is that massive Twotinos—objects having a few times Pluto’s mass—can deplete the two islands differentially (Tiscareno & Malhotra 2003; Tiscareno 2004). Such large objects either have yet to be discovered or were ejected early in the history of the solar system.

4.2. Observational Biases

⁹ Capture is certain if the separatrix dividing circulation and symmetric libration forms outside of the circulation trajectory occupied by the particle and probabilistic if this separatrix forms inside the circulation trajectory (see, e.g., Peale 1986).

¹⁰ Chapter 23 on random Bernoulli trials contains typos in the formulae for dP/du .

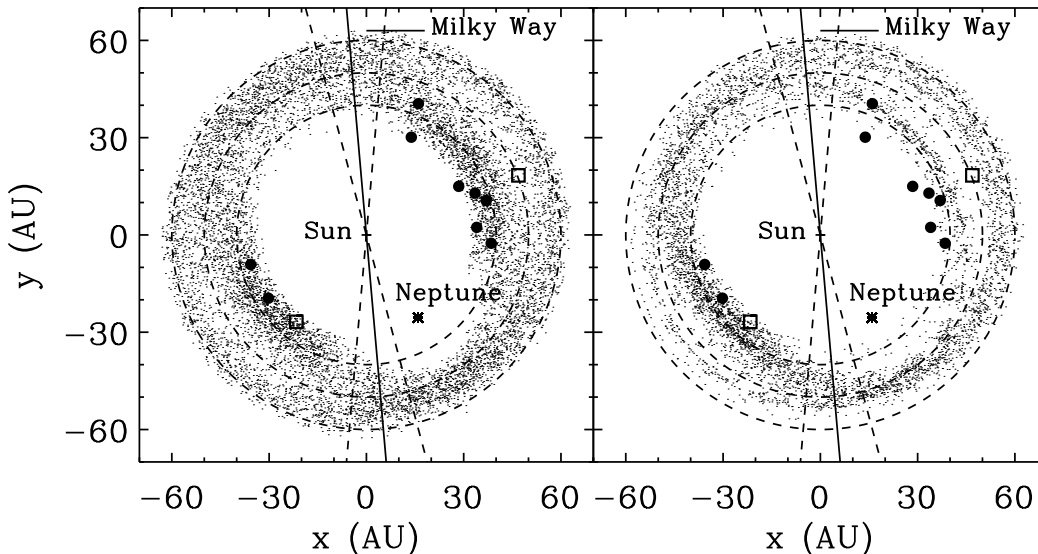


FIG. 17.— Current positions of 11 known Twotinos discovered by surveys world-wide. Of these 11, 2 are symmetric librators (open squares), while 9 are asymmetric librators (solid circles) that we use to constrain Neptune’s ancient migration speed. Overlaid are simulated snapshots of 2:1 resonant objects taken from CJ; the left panel portrays the outcome for an exponential migration timescale of $\tau = 10^7$ yr, while the right panel corresponds to $\tau = 10^6$ yr. Two asymmetric librators lie in the trailing island, while seven lie in the leading island; a de-biased estimate of the population ratio is 3-to-6 and rules out the hypothesis that $\tau \leq 10^6$ yr at 99.65% confidence.

What about observational biases? Since the 3:2 resonance admits no asymmetric libration, Plutinos, unlike Twotinos, have no choice but to be distributed symmetrically about the Sun-Neptune line. For this reason, Plutinos can serve to calibrate detection efficiencies of surveys as a function of orbital longitude. Observationally, 35 Plutinos have been discovered at longitudes leading Neptune and 25 have been discovered at trailing longitudes (see, e.g., figure 14 of CJ). The observed asymmetry is in the same sense as for the Twotinos. If we assume that Plutinos are equally likely to be trailing or leading Neptune, then the probability that the difference in the number of Plutinos found trailing and leading Neptune is ≥ 10 (given a sample size of 60) is 25% according to the binomial distribution. This result does not indicate strongly whether discovering and astrometrically recovering KBOs at longitudes leading Neptune has historically been easier than at trailing longitudes.¹¹ If we assume a bias and use the Plutinos to de-bias the Twotinos, then we estimate a de-biased trailing-to-leading ratio for Twotinos of 3-to-6 (2.6-to-6.4, rounded to the nearest integer). The likelihoods cited above increase to 0.35% ($\tau \leq 10^6$ yr), 17% ($\tau \leq 10^7$ yr), and 39% ($\tau \geq 10^7$ yr). A small increase in the total sample size of 2:1 KBOs could dramatically increase our confidence that fast migration did not occur. We look forward to the advent of the Pan-STARRS synoptic survey with its anticipated discovery of $\sim 10^3$ Twotinos.

5. SUMMARY AND EXTENSIONS

¹¹ Leading longitudes correspond to spring/summer in the Northern hemisphere, and trailing longitudes correspond to fall/winter.

Orbital migration of bodies embedded in disks can explain observed structures in systems ranging from planetary rings to extra-solar planets. As a body migrates, it can capture others into mean-motion resonances, leaving a potentially lasting signature of its migration. In our solar system, numerous Kuiper belt objects (KBOs) exist in mean-motion resonance with Neptune, suggesting that Neptune may have migrated outwards by several AUs (Malhotra 1995; Chiang et al. 2003ab). Chiang & Jordan (2002, CJ) discover by numerical simulation that the subset of KBOs inhabiting the 2:1 resonance furnishes a unique probe of Neptune’s migration history. The resonant angle, ϕ , of such KBOs can librate about values equal to π (symmetric resonance), greater than π (trailing asymmetric resonance), or less than π (leading asymmetric resonance). These authors find that if Neptune’s migration occurred on timescales shorter than 10^7 years (for their assumed initial conditions), more 2:1 resonant KBOs would have been captured into trailing resonance than into leading resonance; as a consequence, more KBOs would be discovered today at longitudes trailing Neptune than at longitudes leading it. For longer timescales of migration, more equal numbers of KBOs would be found leading and trailing Neptune. Observational confirmation of more trailing than leading KBOs in 2:1 resonance would constitute strong evidence in favor of the (fast) migration hypothesis; while current tallies are more consistent with equal populations, a definitive census should be possible with the upcoming Pan-STARRS survey.

We have explained the physical origin of this capture asymmetry within the context of the circular, restricted, three-body problem. Asymmetric libration in the 2:1 resonance occurs as a result of the superposition of the direct and indirect components of the planet’s perturbing

acceleration (see also Frangakis 1973; Pan & Sari 2004). The direct component, produced by the direct gravitational attraction between Neptune and the KBO, serves to accelerate the longitude of conjunction (ϕ) toward π . The indirect component arises from changes in the acceleration of the KBO by the Sun brought about by the latter's reflex motion induced by Neptune. This acceleration, whose effect on the KBO's orbit depends only on the difference between the true longitudes of Neptune and of the KBO, accelerates ϕ toward 0 over a synodic period. Thus, the indirect and direct perturbations can counter-balance each other to produce asymmetric libration of ϕ about angles intermediate between 0 and π , and intermediate between π and 2π .

When employing a literal series expansion of the disturbing potential, the inclusion of an inappropriate number of terms can cause spurious asymmetric resonances to appear. For the 2:1 resonance, asymmetric libration is represented qualitatively well by a literal expansion to second order in ϵ but not by expansions to first, third, or fourth order. The second-order expansion should be regarded as nothing more than a useful fitting formula for the true potential.

Particles caught by an outwardly migrating 2:1 resonance fall first into symmetric libration before evolving to asymmetric libration. At the time of transition from symmetric to asymmetric resonance, if the value of ϕ for a particle is larger than a critical angle ψ , then the particle will be caught into the trailing island of asymmetric libration, while if $\phi < \psi$, it will be caught into the leading island. The relative probability that a particle is captured into the trailing rather than the leading island is determined by the fraction of its time spent during symmetric libration at ϕ 's greater than and less than ψ .

Three factors determine this fractional time spent:

1. Migration-induced shifts of the stable and unstable equilibrium points of the resonant potential. Planetary migration shifts the stable points for symmetric and asymmetric resonance to larger values. For asymmetric resonance, migration shifts the unstable point formerly at π , to a smaller value, $\psi < \pi$. Analytic theory informs us that the angular offsets of the stable point of symmetric libration and of the unstable point of asymmetric libration vary inversely with migration timescale, $T_m = a_N/\dot{a}_N$. The greater the shifts, the more likely it is that particles spend more time in symmetric resonance at $\phi > \psi$ and are captured into the trailing island. If the sum of both shifts exceeds the amplitude of symmetric libration—true if $T_m \lesssim T_{m,\text{crit}} \sim 10^7$ yr—preference for capture into the trailing island is overwhelming.
2. Initial particle eccentricity. The influence of migration-induced shifts is greatest when the amplitude of symmetric libration is smallest; the latter demands small particle eccentricities in circulation prior to capture. Analytic theory also tells us that the magnitudes of the shifts themselves grow with smaller eccentricities.
3. Uneven libration rates during symmetric libration. The relative time spent is also affected by differences in $\dot{\phi}$ over one period of symmetric libration.

The average libration rate at $\phi < \psi$ is lower than at $\phi > \psi$ because the close juxtaposition of two equilibrium points at $\phi < \psi$ flattens the potential there. The difficulty with which a particle traverses the turning point at $\phi < \psi$ counteracts the effect of migration-induced shifts and can even reverse the usual sense of the capture asymmetry for large T_m , but not in a way that gives the leading island more than a 2-to-1 advantage over the trailing island in attracting occupants.

We confirm the results of CJ that the migration timescales necessary to capture more particles into the trailing than the leading island are between about 10^6 and 10^7 yr. For T_m shorter than 10^6 yr, the resonance becomes increasingly unable to capture particles at all. For a realistic migration prescription (e.g., an exponential prescription such as Equation 29), Neptune's migration rate decreases with time, so particles beginning at smaller semi-major axes are captured while Neptune is migrating more quickly and are more likely to exhibit asymmetric capture. The final asymmetry in the longitudes of the particles is sensitive to their initial semi-major axes and, more significantly, their initial eccentricities.

Asymmetric libration is not unique to the 2:1 resonance (e.g., Message 1958; Frangakis 1973; Beaugé 1994; Malhotra 1996; Winter & Murray 1997; Pan & Sari 2004). In a $p:1$ exterior resonance, the resonant angle,

$$\phi = p\lambda - \lambda_N - (p-1)\varpi, \quad (35)$$

can librate asymmetrically as well. For all other resonances, including interior resonances (e.g., 1:2), asymmetric resonance does not occur. Asymmetric libration of the type exhibited by the 2:1 resonance requires a non-zero indirect acceleration. We prove below that the indirect acceleration always averages to zero over one synodic period for a $p:q$ resonance except when $q = 1$, where $p > q$ refers to an exterior resonance and $p < q$ to an interior resonance ($p \neq q$ are relatively prime, positive integers). The order of the resonance is $s = |p - q|$, and the resonant angle is $\phi = p\lambda - q\lambda_N - (p - q)\varpi$. Our proof is essentially identical to that of Frangakis (1973), and derived independently; we offer our expanded version for ease of reference.

The azimuthal component of the indirect acceleration of the KBO by Neptune equals $-(Gm_N/a_N^2)\sin\Delta\theta$, where $\Delta\theta \equiv \lambda_N - f - \varpi$ is the angle between the true longitudes of the planet and of the particle. The proof for the radial component reads completely analogously. Over one synodic period, the tangential acceleration time-integrates to

$$\begin{aligned} \langle T \rangle &= -\frac{Gm_N}{a_N^2} \oint \sin(\lambda_N - f - \varpi) dt \\ &= -\frac{Gm_N}{a_N^2} \int_0^{2\pi s} \frac{\sin(\Delta\theta)}{n_N - \dot{f}(\Delta\theta) - \dot{\varpi}} d(\Delta\theta). \end{aligned} \quad (36)$$

After one full period of the particle, the particle returns to the same true longitude while the planet increases its true longitude by $2\pi s/q$, increasing $\Delta\theta$ by $2\pi s/q$. It follows that $\dot{f}(\Delta\theta)$ is periodic in $\Delta\theta$ with period $2\pi s/q$, as is any function of \dot{f} , including

$$F(\Delta\theta) \equiv \left[n_N - \dot{f}(\Delta\theta) - \dot{\varpi} \right]^{-1}, \quad (37)$$

which may be Fourier-decomposed as

$$F(\Delta\theta) = \frac{b_0}{2} + \sum_{j=1}^{\infty} b_j \cos\left(\frac{j\pi}{L}\Delta\theta\right) + \sum_{j=1}^{\infty} c_j \sin\left(\frac{j\pi}{L}\Delta\theta\right), \quad (38)$$

where $2L \equiv 2\pi s/q$. We have neglected the tiny variation of $\dot{\omega} \ll n_N$ over a synodic period. Plugging this expression for F into Equation 36, we find

$$\begin{aligned} \langle T \rangle &= -\frac{Gm_N}{a_N^2} \int_0^{2\pi s} F(\Delta\theta) \sin(\Delta\theta) d(\Delta\theta) \\ &= -\frac{Gm_N}{a_N^2} \left[s \sum_{j=1}^{\infty} b_j \int_0^{2\pi} \cos(jqx) \sin(sx) dx + \right. \\ &\quad \left. s \sum_{j=1}^{\infty} c_j \int_0^{2\pi} \sin(jqx) \sin(sx) dx \right] \\ &= -\frac{Gm_N}{a_N^2} s\pi \sum_{j=1}^{\infty} c_j \delta_{(jq)s}. \end{aligned} \quad (39)$$

Thus, $\langle T \rangle \neq 0$ only when $jq = s = |p - q|$ for some j . This is satisfied only when $q = 1$ and $j = |p - q|$ under our assumption that p and q are relatively prime.¹² We conclude that asymmetric libration, of the kind exhib-

¹² When q is even, one can see that the indirect term integrates to zero by appealing to diagrams analogous to Figure 3 and noting symmetry over the synodic period.

¹³ The only resonance for which our proof does not apply is the 1:1 resonance. But it is clear that the indirect acceleration does not

ited by the 2:1 resonance, can only exist for exterior $p:1$ resonances.¹³

Future theoretical work should focus on determining the degree of stochasticity in migration driven by scattering planetesimals, and on the size spectrum of planetesimals required for resonance capture to proceed smoothly. We have made preliminary estimates which suggest that for a Neptune-mass disk in the vicinity of Neptune, the disk mass must be concentrated in planetesimals whose sizes do not exceed ~ 100 km for the theory that we have described in this paper to apply. Reasons to imagine that planetesimal sizes were small can be found in the review of planet formation by Goldreich et al. (2004).

We thank Re'em Sari and Margaret Pan for pointing out the importance of the indirect term early in our investigation of asymmetric resonance. Renu Malhotra provided a referee's report that helped to improve the presentation of this paper and that spurred us to greater insights. We are grateful to Joe Hahn, David Jewitt, Alessandro Morbidelli, and Mark Wyatt for stimulating discussions. R.A.M. acknowledges support by a National Science Foundation (NSF) Graduate Fellowship. E.I.C. acknowledges support by NSF Grant AST 02-05892 and the Alfred P. Sloan Foundation.

time-average to zero in tadpole and horseshoe orbits, which may be regarded as asymmetric and symmetric librations, respectively. See Frangakis (1973) and Pan & Sari (2004).

REFERENCES

- Beaugé, C. 1994, *Celestial Mechanics and Dynamical Astronomy*, 60, 225
 Borderies, N., & Goldreich, P. 1984, *Celest. Mech.* 32, 127
 Buie, M.W., et al. 2003, *Earth, Moon, and Planets*, 92, 113
 Chiang, E.I., & Jordan, A.B. 2002, *AJ*, 124, 3430 (CJ)
 Chiang, E.I., et al. 2003a, *AJ*, 126, 430
 Chiang, E.I., et al. 2003b, *Earth, Moon, and Planets*, 92, 49
 Elliot, J.L., et al. 2004, *AJ*, submitted
 Fernandez, J.A., & Ip, W.H. 1984, *Icarus*, 58, 109
 Frangakis, C.N. 1973, *ApSS*, 22, 421
 Goldreich, P. 1965, *MNRAS*, 130, 159
 Goldreich, P., Lithwick, Y., & Sari, R. 2004, *ARA&A*, 42, 549
 Hahn, J.M., & Malhotra, R. 1999, *AJ*, 117, 3041
 Henrard, J. 1982, *Celest. Mech.*, 27, 3
 Lee, M.H., & Peale, S.J. 2002, *ApJ*, 567, 596
 Malhotra, R. 1995, *AJ*, 110, 420
 Malhotra, R. 1996, *AJ*, 111, 504
 Marcy, G., et al. 2001, *ApJ*, 555, 418
 Message, P.J. 1958, *AJ*, 63, 443
 Murray, C.D., & Dermott, S.F. 1999, *Solar System Dynamics* (Cambridge: Cambridge University Press)
 Murray, N., et al. 1998, *Science*, 279, 69
 Pan, M., & Sari, R. 2004, *AJ*, 128, 1418
 Peale, S.J. 1986, in *Satellites*, eds. J.A. Burns & M.S. Matthews (Tucson: Univ. Arizona Press), 159
 Port, S.C. 1994, *Theoretical Probability for Applications* (New York: John Wiley & Sons, Inc.)
 Press, W.H., Teukolsky, S.A., Vetterling, W.T., & Flannery, B.P. 1992, *Numerical Recipes in C. The Art of Scientific Computing* (Cambridge: University Press)
 Thommes, E.W., Duncan, M.J., & Levison, H.F. 1999, *Nature*, 402, 635
 Thommes, E.W., Duncan, M.J., & Levison, H.F. 2002, *AJ*, 123, 2862
 Tiscareno, M.S. 2004, Ph.D. Thesis, University of Arizona
 Tiscareno, M.S., & Malhotra, R. 2003, *DPS Meeting #35, #39.22*
 Ward, W. 1997, *ApJ*, 482, L211
 Winter, O.C., & Murray, C.D. 1997, *A&A*, 328, 399
 Wyatt, M.C. 2003, *ApJ*, 598, 1321